Spintronic effects and devices in nonlinear optics ⊕

Gil Bashan ⓘ ; Shani Izhak ⓘ ; Ofir Yesharim ⓘ ; Ady Arie ✉ ⓘ

Check for updates

View Online   Export Citation

Articles You May Be Interested In

A unifying perspective on non-stationary kernels for deeper Gaussian processes

APL Mach. Learn. (February 2024)

Microstructured optical fibers for quantum applications: Perspective

Unfolding the prospects of computational (bio)materials modeling

J. Chem. Phys. (September 2020)

Spintronic effects and devices in nonlinear optics

View Online   Export Citation   CrossMark

Gil Bashan, (iD) Shani Izhak, (iD) Ofir Yesharim, (iD) and Ady Arie[a] (iD)

AFFILIATIONS

School of Electrical Engineering, Fleischman Faculty of Engineering, Tel Aviv University, Tel Aviv, Israel

[a]Author to whom correspondence should be addressed: ady@tauex.tau.ac.il

ABSTRACT

In this perspective article, we discuss the analogy between spin transport in magnetization texture and the nonlinear process of sum frequency generation, where the signal and idler complex amplitudes represent the two-dimensional spinor, while the nonlinear coupling represents the material magnetization. This analogy unveils new nonlinear optical effects in both spatial and temporal domains, including the analog of the famous Stern–Gerlach effect, the topological Hall effect in magnetic skyrmion structures, and the transverse localization of spin currents in a disordered magnetic spin-glass phase. Moreover, it enables us to realize new all-optical devices that manipulate superposition states of the signal and idler. Examples include a pump-controlled spin valve, which can either reflect or transmit the signal-idler waves when they are in-phase, and a spin waveguide that guides only in-phase signal-idler waves.

13 January 2025 16:48:01

I. INTRODUCTION

Nonlinear optics is used nowadays in numerous applications, including the frequency conversion of coherent light sources into spectral regimes in which compact and efficient lasers are not available, the generation of non-classical states of light such as entangled photon pairs and squeezed light, phase-sensitive parametric amplification, and more. Nonlinear interactions are typically categorized based on the type of nonlinearity of the material. Second-order nonlinear interactions, such as second harmonic generation, sum- (SFG) and difference-frequency generation, and spontaneous parametric down-conversion, utilize $\chi^{(2)}$, the second-order susceptibility tensor of the material. These processes exist only in a rather small class of non-centro-symmetric materials. In contrast, third-order nonlinear interactions, such as for example, third harmonic generation or spontaneous four-wave mixing, can occur in every material by utilizing $\chi^{(3)}$, the third-order susceptibility tensor.

For efficient nonlinear processes, the total energy and momentum of the interacting light waves should be maintained. Traditionally, nonlinear interactions are analyzed by the so-called coupled wave equations (CWEs),[1] which describe the rate of change of the amplitude of each of the interacting waves, with respect to either the propagation spatial coordinate or the time coordinate. However, in recent years, a new approach was introduced for analyzing these

interactions, particularly for the case of three-wave mixing with one strong (hence nearly non-depleted) pump wave,[2,3] or alternatively for the case of four-wave mixing (FWM) with two strong and nearly non-depleted pump waves.[4] In these cases, only the two remaining waves, traditionally called signal and idler waves, exchange energy, and the dynamics are that of a two-level system. This is the same dynamical behavior that occurs for many other systems, such as two coupled mechanical pendula, a two-level atom coupled by an electromagnetic field, a spin-1/2 particle in an external magnetic field, two coupled waveguides, and more. Moreover, many tools and concepts that were developed in those analogous systems can now be implemented to study nonlinear optical interactions. These include, for example, a geometrical representation of the state and the dynamics on a Bloch sphere,[2] eigenvalue diagrams,[3,5] accumulation of geometric phase in nonlinear interaction,[6–9] broadband adiabatic frequency conversion (the nonlinear optics analog of rapid adiabatic passage in atomic physics),[2,3,10] and more.

Specifically, in this article, we explore the analogy between the nonlinear optical interaction and the interaction of spin-1/2 in an external magnetic field. As will be shown in Sec. II, the CWEs can be written analogously to the well-known Pauli equation, which describes spin dynamics in a weak transverse magnetic field. In this case, the spin analog is a 2 × 1 vector of the complex amplitudes of the signal and idler waves, and the effective magnetic field,

or magnetization, is given by the nonlinear coupling. This enables the realization, via nonlinear optics, of the all-optical Stern–Gerlach effect.

In the original Stern–Geralch experiment,[11] silver atoms were split into two distinct directions by a transversely varying magnetic field, depending on the state of the spin of the valence electrons in that atom. Similarly, using the aforementioned analogy, it is possible to show that light beams or light pulses can be split either in space or in time by varying the nonlinear coupling, depending on the relative phase between the signal and idler fields. This will be discussed in detail in Sec. III A. Other interesting effects that will be reviewed here include the transverse localization of spin currents in disordered nonlinear material[12,13] (Sec. III B) and the topological Hall effect in optical magnetic skyrmions[14] (Sec. III C).

Moreover, we describe a new class of optical devices that exhibit different responses for in-phase signal and idler waves ("spin up") compared to out-of-phase signal and idler waves ("spin down"). These include a pump-controlled spin valve device[15] (Sec. III D) that either reflects or transmits the in-phase signal-idler waves, a spin beamsplitter that transmits the in-phase signal-idler waves while reflecting the out-of-phase signal-idler waves,[15] and a spin waveguide that guides only in-phase signal-idler waves[16,17] (Sec. III E). A short summary and suggestions for future work are discussed in Sec. IV.

From a broader perspective, the analogies discussed in this perspective article form the basis for a new venue for an experimental platform to emulate spin physics. It enjoys the widely accessible platform of nonlinear optics (or other optical systems as discussed below). This in turn offers new avenues for controlling various degrees of freedom, such as wavelength and polarization, with promising prospects for high-speed all-optical control.

II. THEORETICAL ANALYSIS

Assuming the approximations of slowly varying envelopes and non-depleted pump, the CWEs governing the SFG process in second-order nonlinearity can be expressed in general as follows:

$$i\frac{\partial A_i}{\partial z} + \left(\frac{\nabla_T^2}{2k_i} - \frac{\beta_{2i}}{2}\frac{\partial^2}{\partial \tau^2}\right)A_i = -\frac{4d_{eff}\omega_i^2}{2k_ic^2}A_p^*A_se^{-i\Delta k'z},$$
$$i\frac{\partial A_s}{\partial z} + \left(\frac{\nabla_T^2}{2k_s} - \frac{\beta_{2s}}{2}\frac{\partial^2}{\partial \tau^2}\right)A_s = -\frac{4d_{eff}\omega_s^2}{2k_sc^2}A_pA_ie^{+i\Delta k'z}. \quad (1)$$

Here, A_j, k_j, and ω_j with $j = s, i, p$ (for signal, idler, and pump, respectively) are the slowly varying complex envelope, wavenumber, and angular frequency for each of the interacting fields. $\nabla_T^2 = \frac{\partial^2}{\partial x^2} + \frac{\partial^2}{\partial y^2}$ is the transverse Laplacian, where x and y are the transverse axes, β_{2s} and β_{2i} are the dispersion coefficients of the signal and idler, respectively, d_{eff} is the effective second-order nonlinear coefficient, and c is the speed of light in vacuum. The propagation axis is denoted by z and $\tau = t - \frac{z}{v_g}$ is the time in a reference frame moving at the group velocity, v_g, of the waves. The wave number mismatch is $\Delta k' = k_p + k_i - k_s$ and stems from material dispersion. To reduce phase mismatch and obtain an efficient nonlinear process, the quasi-phase matching technique is commonly used.[1,18] In this technique, the nonlinear medium is spatially modulated and can be expressed by a Fourier series: $d(z) = \sum_j d_j \exp(iq_jz)$. Assuming that only the

first-order term in the Fourier series phase-matches the interaction, the effective wave number mismatch becomes $\Delta k = k_p + k_i - k_s - q_1$, where q_1 is the effective wave number of the crystal [see Fig. 1(a)], and the magnitude of the nonlinear terms in the case of periodic modulation with 50% duty cycle is $d_{eff} = d_1 = \frac{2}{\pi}d_{mn}$, where d_{mn} is the relevant component of the second-order susceptibility tensor, $\chi^{(2)}$. The two terms in brackets on the left-hand side of Eq. (1) represent diffraction and dispersion, respectively. In the case of continuous waves (CW), the dispersion term is neglected, while in waveguides, the diffraction term is ignored.

For third-order nonlinearity in an FWM process, the general form of the CWEs under the approximations of slowly varying envelopes and non-depleted pumps includes both dispersion and diffraction terms. However, in an optical waveguide, the CWEs can be simplified to

$$i\frac{\partial A_i}{\partial z} - \frac{\beta_{2i}}{2}\frac{\partial^2}{\partial \tau^2}A_i = -2\gamma A_sA_{p1}A_{p2}^*e^{j\Delta kz},$$
$$i\frac{\partial A_s}{\partial z} - \frac{\beta_{2s}}{2}\frac{\partial^2}{\partial \tau^2}A_s = -2\gamma A_iA_{p2}A_{p1}^*e^{-j\Delta kz}. \quad (2)$$

Here, A_{p1} and A_{p2} are the slowly varying complex envelopes of the two pumps, and the wave number mismatch is $\Delta k = k_{p1} + k_i - k_{p2} - k_s$, where k_{p1} and k_{p2} are the wavenumbers of the two pumps [see Fig. 1(b)]. γ is the Kerr nonlinear coefficient and is expressed in units of $W^{-1}\,m^{-1}$.

By introducing normalized fields in the rotating frame, $\psi_{i/s} = \left(|A_i|^2 + |A_s|^2\right)^{-1/2}\exp\left(\mp\frac{i\Delta kz}{2}\right)A_{i/s}$, the CWEs for either SFG or FWM processes, with dispersion or diffraction, can be written in a matrix form with a position-independent coupling matrix:

$$i\frac{\partial}{\partial z}\begin{pmatrix}\psi_i \\ \psi_s\end{pmatrix} = \left(C_1\mathbf{p}^2 - \boldsymbol{\sigma}\cdot\mathbf{M}\right)\begin{pmatrix}\psi_i \\ \psi_s\end{pmatrix}. \quad (3)$$

In Eq. (3), C_1 is either $1/2k$ or $-\beta_2/2$ for SFG and FWM processes, respectively, $\mathbf{p}$ represents the effective momentum operator, $\sigma = (\sigma_x, \sigma_y, \sigma_z)$ is the Pauli matrix vector, and $\mathbf{M}$ is the synthetic magnetization vector, defined as follows:

$$\mathbf{M} = M_0\left(\hat{\mathbf{x}}\cos(\phi) + \hat{\mathbf{y}}\sin(\phi)\right) + \hat{\mathbf{z}}\frac{\Delta k}{2}, \quad (4)$$

with M_0 and ϕ are defined in Table I. Equation (3) is mathematically analogous to the transverse Pauli equation, which models the behavior of a non-relativistic spin-1/2 particle under the influence of a weak transverse magnetic field.[19] The specific interpretation of Eqs. (3) and (4) depends on whether it pertains to SFG or FWM with dispersion or diffraction. These scenarios are summarized in Table I, where we approximate $k_i \approx k_s = k$ due to the long-wavelength pump approximation. In the case of FWM, we assume that the two pumps have similar wavelengths; hence, $\beta_{2i} \approx \beta_{2s} = \beta_2$.

This analogy can be geometrically visualized on a frequency-domain Bloch sphere, where $\psi = \begin{pmatrix}\psi_i \\ \psi_s\end{pmatrix}$ represents the effective pseudospin state vector of the system.[2,9,20] In this representation, the idler and signal frequencies correspond to the north and south poles of the Bloch sphere, respectively. The equator hosts equal superpositions of the signal and idler frequencies, while any other point on the
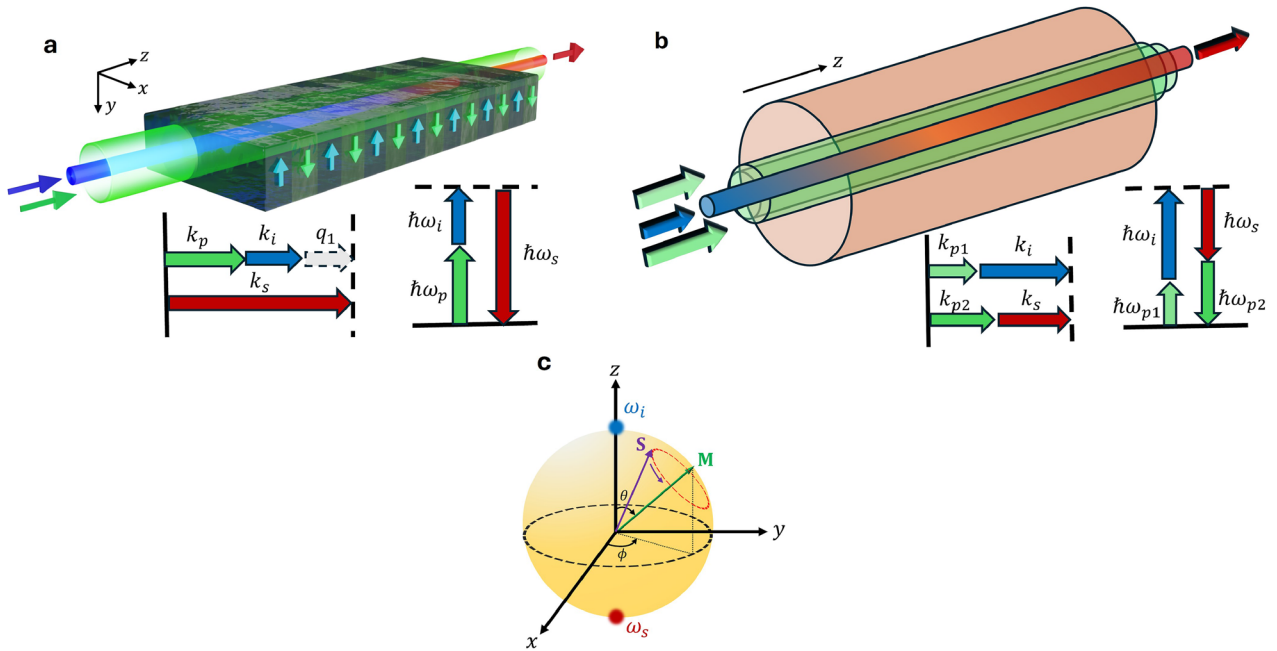
FIG. 1. Illustration of nonlinear optical processes. (a) An SFG process: a pump (in green) and idler (in blue) interact within a nonlinear photonic crystal to generate the signal (in red). Quasi-phase matching is used to achieve phase matching. The momentum conservation and energy conservation requirements are shown in the inset. (b) An FWM process in an optical fiber: two pump beams together with an idler beam (in blue) generate the signal (in red), with phase matching naturally satisfied. The momentum conservation and energy conservation requirements are shown in the inset. (c) Frequency-domain Bloch sphere: the state vector **S** processes along a circle around the magnetization vector, **M**. The z component of the magnetization vector is controlled by the momentum mismatch, Δk, with θ denoting the elevation angle. The radial component of **M** is defined by the nonlinear coupling strength, M_0, and its radial direction is defined by ϕ, the azimuthal angle, given by the relative phase between the poling phase and pump phase front or between the two pump wavefronts, depending on whether we employ the SFG or FWM frameworks, respectively.

TABLE I. The physical parameters of SFG and FWM nonlinear processes, under the non-depleted pump approximation, considering both diffraction and dispersion effects. ϕ_p, ϕ_{p1}, and ϕ_{p2} are the phases of the pumps, and ϕ_{NLPC} is the modulation phase of the nonlinear photonic crystal (NLPC).

	SFG		FWM	
	Dispersion	Diffraction	Dispersion	Diffraction
C_1	$-\beta_2/2$	$1/2k$	$-\beta_2/2$	$1/2k$
Effective momentum operator, p	$-i\frac{\partial}{\partial\tau}$	$-i\nabla_T$	$-i\frac{\partial}{\partial\tau}$	$-i\nabla_T$
Synthetic magnetization magnitude, M_0	$\frac{2|d_{\text{eff}}A_p|k}{n_i n_s}$	$\frac{2|d_{\text{eff}}A_p|k}{n_i n_s}$	$4|\gamma A_{p1}A_{p2}^*|$	$4|\gamma A_{p1}A_{p2}^*|$
Synthetic magnetization phase, ϕ	$\phi_p - \phi_{\text{NLPC}}$	$\phi_p - \phi_{\text{NLPC}}$	$\phi_{p2} - \phi_{p1}$	$\phi_{p2} - \phi_{p1}$
Temporal/transverse axis, ζ	τ	x	τ	x
Fourier axis, ξ	ω	k_x	ω	k_x
Sign, C_2	-1	1	-1	1

surface represents a state vector with different signal and idler populations and relative phases. The dynamics between the signal and idler fields during the nonlinear interaction can then be described as the precession of the Bloch vector, $S = \psi^\dagger \sigma \psi$, along a circle around the synthetic magnetization vector **M**, according to the following equation:[2,9]

$$\frac{\partial}{\partial z}\mathbf{S} = \mathbf{M} \times \mathbf{S}. \tag{5}$$

In terms of field amplitudes, $S_x = \frac{1}{N}\sqrt{\frac{n_i n_s}{\omega_i \omega_s}} 2\text{Re}\left(e^{-i\Delta kz/2}A_i^* A_s\right)$, $S_y = \frac{1}{N}\sqrt{\frac{n_i n_s}{\omega_i \omega_s}} 2\,\text{Im}\left(e^{-i\Delta kz/2}A_i^* A_s\right)$, and $S_z = \frac{1}{N}\left(\frac{n_i}{\omega_i}|A_i|^2 - \frac{n_s}{\omega_s}|A_s|^2\right)$. In addition, the magnitude $|\mathbf{S}| = \sqrt{S_1^2 + S_2^2 + S_3^2}$ is equal to 1 for a system in a pure state and <1 for a system in a mixed state. This geometrical representation, as well as the precession of the Bloch vector around the synthetic magnetization vector, is illustrated in Fig. 1(c).

Assuming phase-matched processes, that is, $\Delta k = 0$, the synthetic magnetization vector, $\mathbf{M}$, is purely transverse with $\mathbf{M} = \mathbf{M}_T = M_0(\hat{\mathbf{x}}\cos(\phi) + \hat{\mathbf{y}}\sin(\phi))$. For the Stern–Gerlach experiment, we set the synthetic magnetization near half of the maximal value, so that it can be linearly approximated as $|\mathbf{M}| = M_1 + \zeta M'$, where $M_1 \approx M_0/2$. Namely, a gradient in the synthetic magnetization is present. Equation (3) can be diagonalized in the Fourier space, resulting in two eigenstates:

$$|\psi_\pm\rangle = \frac{|\psi_s\rangle \pm e^{-i\phi}|\psi_i\rangle}{\sqrt{2}}. \tag{6}$$

The spinor as a function of propagation coordinate z can be expressed using the effective propagator, $\exp(-izH_\pm)$, as $|\psi\rangle(z,\omega) = (\exp(-izH_+)|\psi_+\rangle\langle\psi_+| + \exp(-izH_-)|\psi_-\rangle\langle\psi_-|)\psi_{\text{incident}}$, where $H_\pm = -C_1\omega^2 \mp M_1 \mp iC_2M'\frac{\partial}{\partial\xi}$ represents the two effective Hamiltonians corresponding to the two eigenstates given in Eq. (6).[21] The effective propagator can be computed using the Zassenhaus formula:

$$\exp(-izH_\pm) = \exp\left(\pm izM_1 - \frac{i}{3}C_1C_2z^3(M')^2\right)\exp\left(\mp zC_2M'\frac{\partial}{\partial\xi}\right)$$
$$\times \exp(-izC_1\xi^2 \mp iC_1C_2z^2M'\xi). \tag{7}$$

Here, the term $\exp\left(\mp zC_2M'\frac{\partial}{\partial\xi}\right)$ serves as the translation operator in the ξ dimension, while the term $\exp(\mp iC_1C_2z^2M'\xi)$ introduces a shift along the ζ axis, with the direction varying according to the eigenstates. Both of these correspond to the nonlinear optical Stern–Gerlach effect in either time or space. The term $\exp(\pm izM_1)$ represents distinct phase accumulations for each eigenstate, which can lead to Rabi oscillations between the signal and the idler, a characteristic phenomenon of two-level systems. These oscillations arise from the interference between the two eigenstates. Therefore, when the incident spinor is a pure eigenstate, no oscillations occur. The term $\exp(-izC_1\xi^2)$ is directly related to diffraction or dispersion, and the term $\exp\left(-\frac{i}{3}C_1C_2z^3(M')^2\right)$ represents a phase that is cubic in z and quadratic in M', commonly referred to as the Kennard phase.[22–24]

III. SPINTRONIC EFFECTS AND DEVICES

The above analogy between spin transport in 2D magnetic materials and the dynamics of the signal and idler fields within a quasi-phase-matched SFG process establishes a controllable optical system for exploring spin transport in complex magnetic materials, which is challenging to investigate in current condensed matter physics techniques. In addition, it opens possibilities for realizing novel spintronic-inspired effects with light. This allows the creation of all-optical devices for controlling and manipulating two-frequency signal-idler light beams, with promising applications in both classical and quantum information processing. In the next sections, we present several examples of such applications.

A. Optical realizations of the Stern–Gerlach effect in space and time

Since the first theoretical work by Karnieli and Arie,[20] there has been a surge in experimental realizations of all-optical Stern–Gerlach effects utilizing the analogy between spin transport

and nonlinear media. The first was published in 2022,[25] where the authors used pump shaping to introduce a linear gradient in the nonlinearity. In this work, using a regular periodically-poled KTP (PPKTP) crystal, an input idler beam was transversely displaced to coincide with the slopes of a wide pump. Then, by increasing the pump power, a clear separation of the generated signal was seen in the far field. In addition, the experiment showed that when a superposition of the signal and idler enters the Stern–Gerlach apparatus, the signal beam does not split but rather remains a single Gaussian lobe, whose deflected angle depends on the relative phase between the generated signal and idler beam, confirming the two-color nature of the interaction. Later, Mondal and Das[26] found that similar dynamics are also present in difference frequency generation. In their experiment, they used optical parametric generation, where a long (50 mm) MgO:PPLN crystal was pumped with an ultrashort pulse. In this work, they used the natural Gaussian beam shape to have a circular, radially changing synthetic magnetization. Similarly to Yesharim et al.,[25] with low pump powers, just a single Gaussian beam was present. When increasing the pump powers, both the signal and idler showed circular splitting from this main lobe, again verifying the two-color interaction [see Fig. 2(a)].

The above experimental results both used quadratic nonlinear processes for the analogy between nonlinear optics and spintronics. Interestingly, several other theoretical and experimental works showed that the same analogy exists in other optical systems. The circular polarization of light beams carries spin angular momentum, and spin-dependent deflection, also known as the spin-Hall effect, can be observed,[28,29] for example, for light that undergoes a helical light trajectory. It is also interesting to note that the dynamics of the system can be described by a Stokes vector precession around an effective magnetic field, in a similar form to Eq. (5). The Spin-Hall effect was also reported in different types of photonic crystals that were designed to exhibit strong spin–orbit coupling.[30,31]

Recently, Liu et al.[27] showed that a similar analogy also exists in an electrically modulated anisotropic medium where the pseudospin constitutes polarized light. There, the synthetic magnetization was induced by a trapezoidal lithium niobate crystal, where the two side faces of the crystal are coated with conductive films to allow the electrical modulation of the refractive index. When circularly polarized light enters the crystal, a simple Gaussian lobe is present at the crystal output facet. When the electrical voltage slowly rises, two distinct lobes exist, showing Stern–Gerlach-type behavior [see Fig. 2(b)]. Interestingly, Liu et al.[27] showed that when the light is structured as a vortex vector beam, the beam can be separated into the constituent wavefronts with different polarizations, therefore acting as a vector beam analyzer.

Similarly, another example of using the electro-optic effect was demonstrated by periodic poling of the electro-optic coefficient by Zhu et al.[32] Then, using electrical voltage, right or left circular input polarized light can be deflected depending on the applied voltage [see Fig. 2(c)]. Importantly, here the pseudospin constitutes equal superposition states of horizontally and vertically polarized light, in contrast to Ref. 27, where the pseudospin constitutes horizontally or vertically polarized light.

Li et al.[33] explored a similar analogy in optically induced waveguides. In their work, they used a photorefractive material (SBN) crystal to induce two optical slab waveguides with a linear coupling between them [see Fig. 2(d)]. Then, structured probe beams were
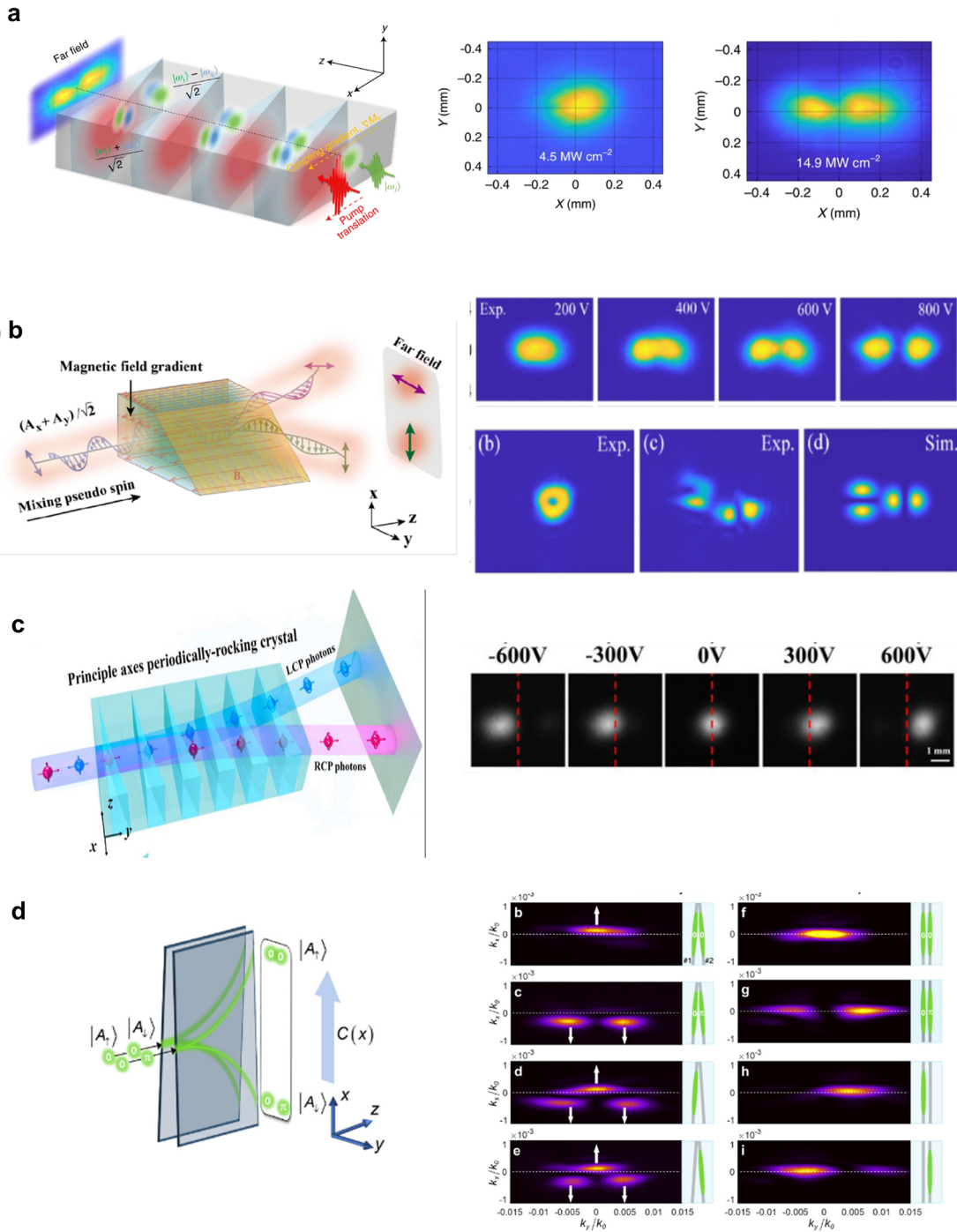
FIG. 2. Experimental realizations of the analogy between the Stern–Gerlach experiment and different optical systems. (a) (left) All-optical Stern–Gerlach effect using SFG. (right) The generated signal beam splits depending on the pump power. (b) Separating horizontally and vertically polarized light using the electro-optic effect. Vortex beams can be analyzed using a higher-order Stern–Gerlach effect (bottom right). (c) Separating right circularly polarized (RCP) and left circularly polarized (LCP) beams using periodic poling of the electro-optic coefficient, depending on the applied voltage. A horizontally polarized beam can be steered left or right depending on the applied voltage (right). (d) Separating waveguide modes in an optically induced linearly varying coupling between two slab waveguides (left). The probe beam can be structured to allow different input pseudospin states, thus changing the output mode structure and angle (right). Panels reproduced with permission from (a) Yesharim *et al.*, Nat. Photonics 16, 582–587 (2022). Copyright 2022 Springer Nature; (b) Liu *et al.*, Optica **11**, 980–987 (2024). Copyright 2024 Optica Publishing Group;[27] (c) Chen *et al.*, Laser Photonics Rev. **18**, 2301030 (2024). Copyright 2024 John Wiley and Sons; (d) Xu *et al.*, Laser Photonics Rev. **18**, 2301055 (2024). Copyright 2024 John Wiley and Sons.

injected inside the photorefractive material. Depending on the relative phase of the excited waveguide modes, the output mode would split (in the case of a superposition) or deflect (in the case of a single spatial mode).

The Stern–Gerlach splitting was demonstrated not only in the spatial/momentum domain but also in the temporal/frequency domain. This was achieved by extending the demonstration of the Stern–Gerlach effect in quadratic nonlinear optics[25,26] to the third-order nonlinearity in optical fibers, as described by Bashan *et al.*[34] Using commercially available telecom components, the authors mixed two pump pulses to induce coupling between the signal and idler pulses via FWM. The pump envelopes were designed to include a linear power ramp that overlapped with the signal and idler pulses, thereby inducing a temporal slope in the synthetic

magnetism [see Fig. 3(a)]. Through coherent detection, the experiment revealed that each system eigenstate [Eq. (6)] was deflected in a different direction within the frequency domain, resulting in eigenstate splitting that varied with the pump pulse power [see Figs. 3(b)-(d)]. In addition, for superposed states, frequency splitting and Rabi oscillations were observed.

B. Pseudospin transverse localization of light in a synthetically disordered nonlinear medium

The spin-glass, a fascinating disordered magnetic phase, features randomly aligned spins due to frustrated interactions,[35–38] resulting in complex magnetic behavior that intrigues multiple scientific disciplines.[35,37,39,40] While theoretical work on spin-glass
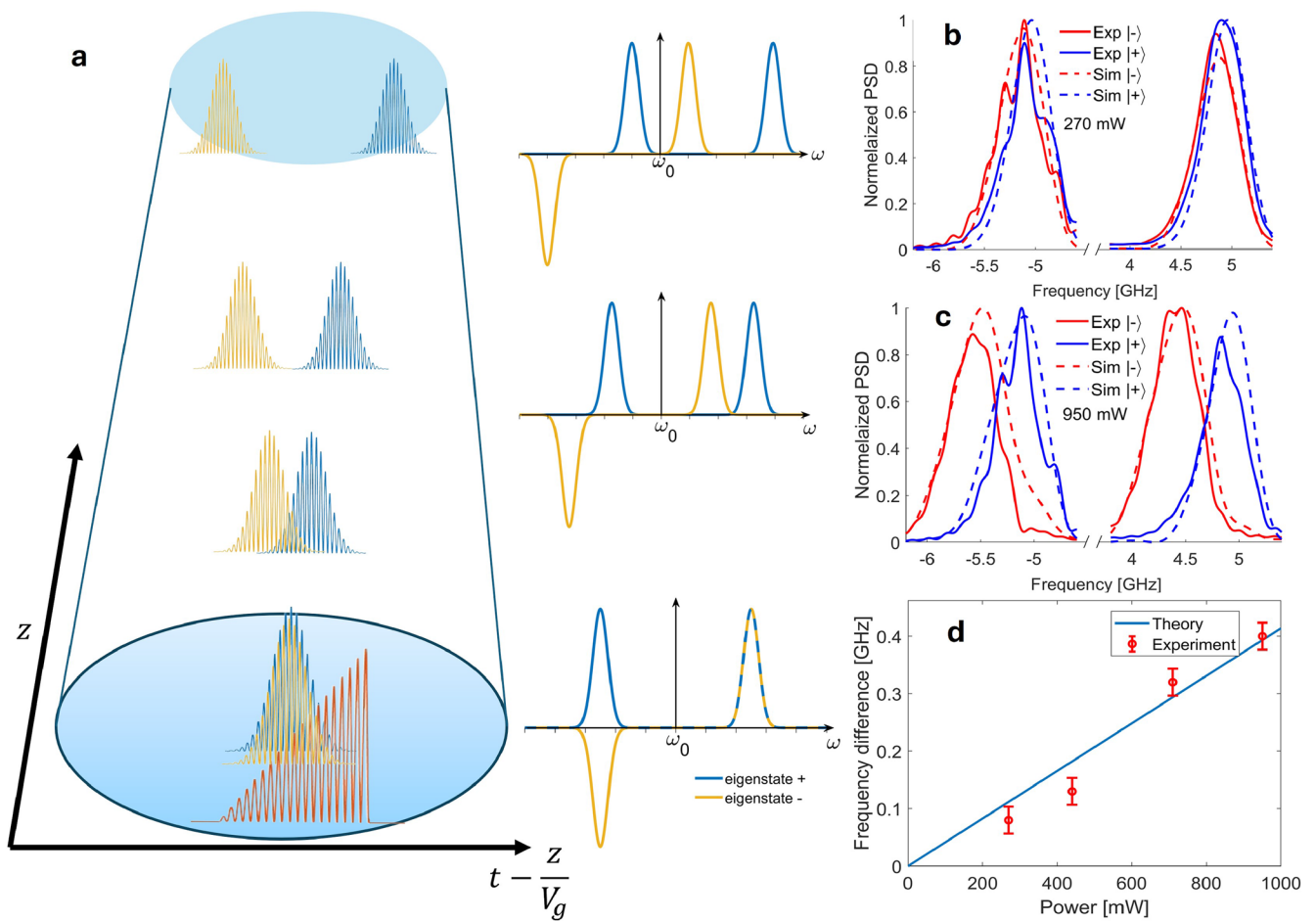

FIG. 3. Temporal Stern–Gerlach effect. (a) Illustration of the all-optical Stern–Gerlach effect in the time domain. Two pump tones within a shared ramped pulse envelope (red) couple light between signal and idler pulses, resulting in two distinct eigenstates (blue and orange), where signal and idler exhibit either the same or opposite phases. As the pulses propagate in the fiber, the eigenstates undergo temporal splitting (left) and frequency splitting (right). (b) Experimental and simulated results of the spectral deflection of the eigenstates' power spectral density. The horizontal axis represents the frequency offset from the carrier, with the signal on the left and the idler on the right. Blue lines represent eigenstate $|\psi_+\rangle$ and red lines represent $|\psi_-\rangle$; solid lines are experimental results and dashed lines are simulations at 270 mW pump peak power, with 0.1 GHz eigenstate frequency offset. (c) As in (b), but with a 950 mW peak power and 0.55 GHz frequency offset. (d) Frequency splitting vs pump peak power, with the solid blue line representing the theoretical model and red markers showing experimental data. Reproduced with permission from Bashan *et al.*, Opt. Express **32**, 9589–9601 (2024). Copyright 2024 Optica Publishing Group.[34]

materials is extensive, experimental investigation of spin current dynamics in these disordered textures has been challenging due to stability issues,[41,42] and the lack of the possibility for coherent control.[42]

In such disordered systems, phenomena like weak localization[43,44] and Anderson localization[45,46] are predicted to occur. Anderson localization, in particular, is a widespread wave phenomenon, where the diffusion of an electron wavefunction halts in the presence of a disordered potential, causing the wavefunction to become spatially localized with exponentially decaying tails. Optics has provided a well-established platform for studying localization, where experiments have pioneered the observation of transverse Anderson localization in 2D[47] and 1D[48] photonic systems, where light becomes localized in the transverse plane with exponentially decaying tails,[49–51] by introducing disordered *scalar* potentials.

By utilizing the aforementioned analogy between an SFG process and spin-1/2 dynamics, spin transport in a disordered spin-glass phase was recently explored, revealing that the signal-idler light beam, acting as the spin current, undergoes transverse localization due to induced disorder in the synthetic magnetization texture.[12,13] Under the assumption of a quasi-phase-matched process, a 2D ordered ferromagnetic material, as illustrated in Fig. 4(a), can be
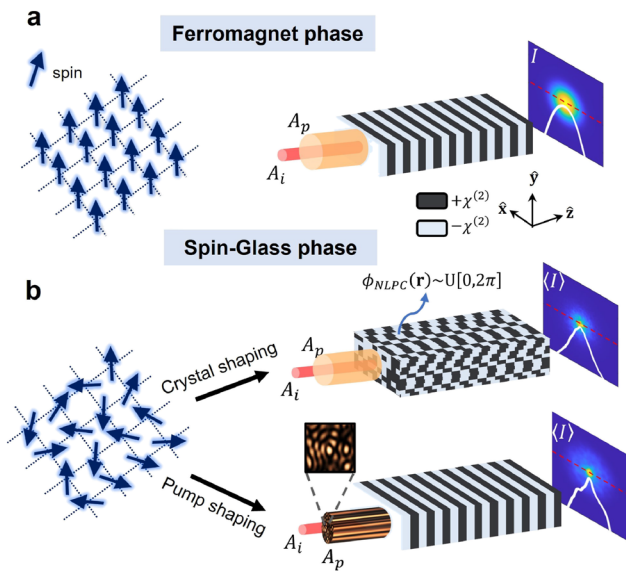
FIG. 4. (a) and (b) Illustrations of the magnetization textures of 2D ferromagnet (a) and spin-glass (b) phases, with their optical analog schemes.[12,13] Spin transport in a ferromagnetic phase is equivalent to Gaussian pump and idler beams impinging on a 1D NLPC, producing a diffracted pseudospin signal-idler beam. This corresponds to a parabolic curve in logarithmic scale (white curve), as calculated along the horizontal red dashed line. Spin transport in a spin-glass phase can be optically emulated using two approaches: [(b), top] Gaussian pump and idler beams impinge on a 3D NLPC with randomly sampled poling phase, or [(b), bottom] a non-diffracting speckled pump with Gaussian idler beams impinging on a 1D NLPC. Both approaches yield a localized pseudospin, as can be seen from the ensemble-averaged output intensity ⟨I⟩, which is now transversely localized, characterized by linear-shaped profiles on a logarithmic scale (white curves), as calculated along the horizontal red dashed lines.

emulated by creating a uniform transverse synthetic magnetization texture. This is optically achieved by employing a 1D periodically poled crystal with a wide, non-depleted Gaussian pump beam. Disorder in the synthetic magnetization texture, mimicking a 2D disordered spin-glass phase, illustrated in Fig. 4(b), can be introduced by shaping either the NLPC parameters or the pump field, as shown in Fig. 4(b). The crystal shaping approach involves sampling the poling phase from a uniform distribution within the range $[0, 2\pi]_x \times [0, 2\pi]_y$, while keeping the pump envelope's phase constant. The pump shaping method involves an all-optical realization of a disordered synthetic transverse magnetization by employing a non-diffracting (ND) speckled pattern as the pump field, a random, propagation-invariant field distribution.

The results presented in Refs. 12 and 13 show that in the optically ordered ferromagnet, a broad Gaussian signal-idler beam emerges at the NLPC's output, indicating dominant diffraction effects. In this case, the intensity distribution follows $I \propto \exp\left(-\frac{2r_T^2}{\sigma^2}\right)$, where $\mathbf{r}_T = (x, y)$ is the transverse position vector and σ denotes the Gaussian beam width, as illustrated in Fig. 4(a). Conversely, when considering the pseudospin transport inside the optical disordered spin-glass, the ensemble-averaged signal-idler output intensity becomes localized in the transverse plane, as shown in Fig. 4(b) (top) and (bottom) for the crystal and pump shaping approaches, respectively. In this case, the optimally fitted curve for the ensemble-averaged signal-idler output intensity profile follows an exponential distribution, $\langle I \rangle \propto \exp\left(-\frac{2|\mathbf{r}_T|}{\xi_{loc}}\right)$, where $|\mathbf{r}_T| = \sqrt{x^2 + y^2}$ represents the transverse distance from the beam's center. The hallmark of localization is evident in the linear-shaped profile on a logarithmic scale in the presence of synthetic disorder, in contrast to the parabolic profile observed in the optical ferromagnet case [white curves in Figs. 4(b) and 4(a), respectively].

These findings, which reveal intriguing properties of spin transport in a disordered magnetic phase, may provide insights into phenomena such as ferromagnetic-metal to glassy-insulator phase transitions,[52–54] while paving the way for exploring challenging phenomena in traditional condensed matter systems. It also opens avenues for discovering novel physical effects in complex magnetic textures, such as spin-ice materials,[41] by tailoring both the nonlinear crystal and the pump beam. In addition, this framework can be adapted to other nonlinear processes, such as difference frequency generation,[26] and third-order nonlinearity,[4,8] and other two-level systems,[27,32,33] potentially uncovering additional intriguing localization effects with light.

C. Skyrmionic nonlinear photonic crystals and the topological Hall effect for light

In 2009, a new form of stable magnetic texture—the skyrmionics lattice—was discovered.[55] This texture consists of magnetic whirl-lines that are topologically robust. When a spin-1/2 particle interacts with the magnetic skyrmion, the topological Hall effect is observed—the particle is deflected either to the left or to the right, depending on the value of the spin. Magnetic skyrmions raised much interest in the research community,[56] and they were proposed for applications such as memory storage and information processing. Moreover, analogies of skyrmion lattices were realized in optics in recent years,[57] where the effective spin texture is formed using

either the electric field components or the spin angular momentum components of surface plasmon polaritons.[58–60] Skyrmion beams can also be formed for freely propagating beams, using either the Stokes vector components of optical beams or the electron spin components of electron beams.[61] Furthermore, skyrmion lattices were recently proposed[62] and experimentally observed[63] with surface water waves. A recent review[57] presents the latest developments in the field of optical skyrmions and outlines several potential applications.

As we have shown in the previous sections, the nonlinear mixing process is analogous to the interaction of a spin-1/2 particle with a magnetization texture, where the effective spinor consists of the complex amplitudes of the signal and idler, and the product of the nonlinear coefficient and the pump field is the effective magnetization. This analogy opens the door to the realization of skyrmionics nonlinear photonic crystals and to the emulation of the topological Hall for light,[14] whereby the signal-idler beam would be deflected either to the left or to the right, depending on the relative phase between the two waves. Owing to the flexibility of modulating the nonlinearity in all three dimensions of the crystals using laser-induced poling,[64] complex skyrmionic structures can be formed. Moreover, the interaction can be all-optically controlled using the pump beam, enabling, for example, control over the direction of the deflection of the signal-idler light beam.

The (normalized) circularly-symmetric space-dependent magnetization texture can be written as

$$\hat{M}(\rho, \phi) = \sqrt{1 - m^2(\rho)}\left[\cos(n\phi + \eta)\hat{\mathbf{x}} + \sin(n\phi + \eta)\hat{\mathbf{y}}\right] + m(\rho)\hat{\mathbf{z}}. \tag{8}$$

Here, ρ, ϕ are the radial and azimuthal polar coordinates. The radial dependence is expressed using $m(\rho)$ in the z direction and $\sqrt{1 - m^2(\rho)}$ in the x–y plane, where $0 \le |m(\rho)| \le 1$, n is the (integer) winding number, and η is a phase factor. To realize the effective magnetization texture in a nonlinear photonic crystal, one needs to vary the poling period and subsequently the phase mismatch (which controls the size of the effective magnetization in the z direction),

as well as the duty cycle and phase that control the magnetization in the x–y plane. In ferroelectric crystals, this requires modulating the nonlinear coefficient in all three dimensions, which is possible by laser-induced poling.[64]

Some interesting magnetization textures include Neel-type skyrmions (or anti-skyrmions), where $m(\rho) = \mp\cos\left(\frac{\pi\rho}{R}\right), n = \pm 1, \eta = 0$:

$$\hat{M}(\rho, \phi) = \sin\left(\frac{\pi\rho}{R}\right)\left[\cos(n\phi)\hat{\mathbf{x}} + \sin(n\phi)\hat{\mathbf{y}}\right] \mp \cos\left(\frac{\pi\rho}{R}\right)\hat{\mathbf{z}}, \tag{9}$$

and Bloch-type skyrmions (anti-skyrmions), where $m(\rho) = \mp\cos\left(\frac{\pi\rho}{R}\right), n = \pm 1, \eta = \frac{\pi}{2}$:

$$\hat{M}(\rho, \phi) = \sin\left(\frac{\pi\rho}{R}\right)\left[-\sin(n\phi)\hat{\mathbf{x}} + \cos(n\phi)\hat{\mathbf{y}}\right] \mp \cos\left(\frac{\pi\rho}{R}\right)\hat{\mathbf{z}}. \tag{10}$$

However, the flexibility of modulating the nonlinear coefficient enables the realization of high-order skyrmions, having $|n| > 1$, and considering other profiles of $m(\rho)$, beyond the above-mentioned cosine dependence on ρ, such as polynomial or exponential functions of ρ^{12}.

When a signal or idler light beam is sent through a nonlinear photonic crystal, having an effective magnetization texture of any of the above-mentioned types of skyrmions, it will exhibit a topological Hall effect, that is, the output beam will be deflected in one direction for the signal and in the opposite direction for the idler. Moreover, as the skyrmion number increases, the deflection angle increases as well. In terms of the propagation dynamics for an SFG process with a non-depleted pump, under the adiabatic condition, the signal-idler spinor will follow the local magnetization. Hence, as shown in Fig. 5, a signal-only beam at the input will be fully converted to an idler-only beam at the center of the skyrmion structure and will be fully converted back to a signal-only beam at the exit plane.

As we discussed in the previous sections, the effective magnetization is a product of the pump wave and the nonlinear modulation of the crystal. So far, we considered the pump as a broad Gaussian beam, but new opportunities emerge when the pump beam
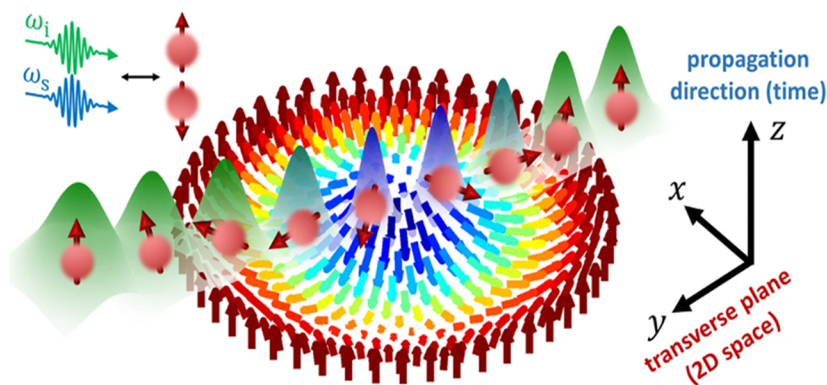

FIG. 5. Dynamics of the pseudospin and position of the light beam as it traverses a synthetic magnetization texture. The propagation coordinate (z) is analogous to the time coordinate, and the location of the light beam on the transverse plane is analogous to the position of the spin-$\frac{1}{2}$ particle (axis inset), while the spin degree of freedom is analogous to the color of the light (green/blue colors representing spin up/down). In a similar manner to the electron spin, adiabatically following the local magnetization direction, light undergoes adiabatic frequency conversion [from green (signal) to blue (idler) and back to green (signal)] as it propagates. Reproduced with permission from Karnieli *et al.*, Nat. Commun. **12**, 1092 (2021). Copyright 2021 Authors, under a Creative Commons license CC BY 4.0.

is structured. Specifically, if we assume a pump beam that carries orbital angular momentum (OAM), the nonlinear modulation pattern becomes much simpler, hence easier to fabricate. In addition, by switching the pump's OAM from a positive value to a negative value, the deflection angle in the topological Hall effect changes sign as well, thus enabling all-optical control of the deflection.

At present, the concept of realizing skyrmion structures using nonlinear photonic crystals has been theoretically and numerically analyzed. An important future challenge is to experimentally realize these structures and observe the corresponding topological Hall effect for light. In addition, it would be interesting to study the nonlinear interaction in the regime of strong signal and idler beams, where the non-depleted pump approximation no longer holds. It is expected that this will reveal new propagation dynamics, similar to spin-transfer torque,[65] in which the magnetization is affected by the spin current.

D. All-optical spin valve effect in nonlinear optics

The spin valve (SV), introduced in the early 1990s,[66] is a fundamental spintronic device extensively utilized in magnetic sensors and magneto-resistive random-access memory technology.[67] The SV consists of "free" and "fixed" ferromagnetic layers separated by a non-magnetic metal layer, as illustrated in Fig. 6(a), and switches between "open" state when the two layers have parallel ("P") magnetization textures, supporting high electric current, and "closed" state when the two layers are anti-parallel ("AP"), with no electric current at all. This switching, based on the giant-magnetoresistance effect, is achieved by applying an external magnetic field that alters the free layer's magnetization relative to the fixed layer.[66]

Leveraging the aforementioned analogy between spin transport and nonlinear optics, an all-optical spin valve device was proposed by Izhak *et al.*,[15] where the signal-idler light beam in a quasi-phase-matched SFG process serves as the spin current, and the synthetic magnetization texture, which determines the device's state, is controlled optically by the pump beam. This configuration allows precise manipulation of the propagation of the signal-idler beam, influenced by the relative phase between the signal and idler fields and by the pump beam's power.

Assuming a quasi-phase-matched process where the synthetic magnetization texture is purely transverse, to emulate the magnetization pattern of a spintronic spin valve, a discontinuity in $\chi^{(2)}(\mathbf{r})$ is introduced, effectively creating two synthetic ferromagnetic layers. This is achieved through a specific poling pattern of the NLPC, in which the poling phase is $\phi_{\text{NLPC}}(\mathbf{r}) = \begin{cases} \pi, & x < 0 \\ 0, & x > 0 \end{cases}$, as depicted in Figs. 6(b) and 6(c), resulting in a synthetic magnetization texture of the form $\mathbf{M}_T(\mathbf{r}) = \begin{cases} -M_0\hat{\mathbf{x}}, & x < 0 \\ +M_0\hat{\mathbf{x}}, & x > 0 \end{cases}$, that can be experimentally realized by electric field poling in ferroelectric nonlinear crystals.

The dynamics of the two-frequency signal-idler pseudospin in this setup are governed by an eigenvalue problem, yielding two orthogonal eigenstates, the frequency-superposition eigenstates $\psi_{\pm}$, defined in Eq. (6). In position-space representation, the evolution of each eigenstate resembles a well-known wave phenomenon in quantum mechanics and electromagnetics—scattering off a step potential, with time evolution replaced by propagation along the optical axis, z:

$$i\frac{\partial}{\partial z}\psi_{\pm} = \left[-\frac{\nabla_T^2}{2\bar{k}} \mp \begin{cases} -M_0, & x < 0 \\ +M_0, & x > 0 \end{cases}\right]\psi_{\pm}. \qquad (11)$$

In this equation, the first term inside the parenthesis represents diffraction, while the second term acts as an effective potential. Specifically, ψ_- encounters an effective step potential, while ψ_+ experiences an effective potential drop, both with a height of $2M_0$ controlled by the pump power, P_{pump}. By adjusting the pump power properly, the device can be switched between two operational modes.[15]

When the pump is off, the device operates in an "open" state, allowing both ψ_- and ψ_+ to pass through the effective potential with high transmission probability. This corresponds to a spintronic spin valve device functioning in its "P" configuration, as depicted in Fig. 6(b). Conversely, when the pump power reaches a specific
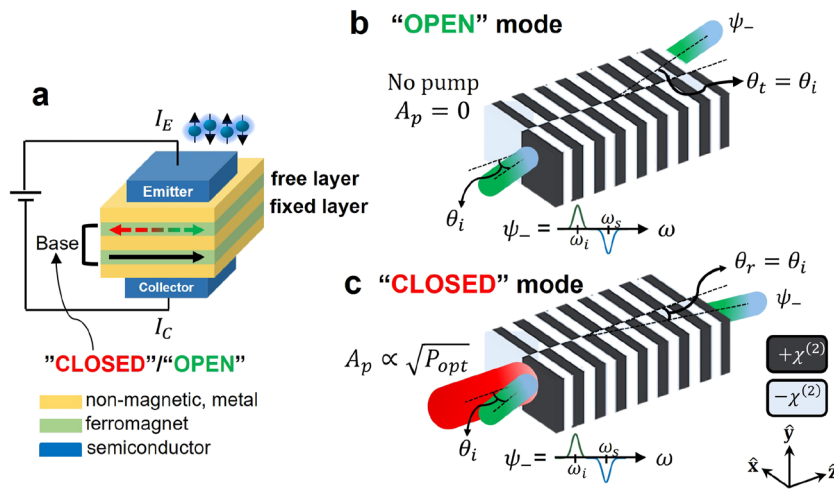

FIG. 6. (a) Illustration of a spintronic SV. The valve is "open" when the ferromagnetic domains in the two layers are parallel ("P") and is "closed" when they are anti-parallel ("AP").[15] (b) and (c) Scheme for realizing an all-optical SV using NLPC. For the spin-down eigenstate as the input optical pseudospin, $\psi_{\text{in}} = \psi_-$, the operation of the device is controlled via the pump power: when $P_{\text{pump}} = 0$ W ($P_{\text{pump}} = P_{\text{opt}}$), the all-optical SV is in an "open" (b) ["closed" (c)] mode and operates in an effective "P" ("AP") configuration, with full light transmission (b) [reflection (c)] along the z-axis of the NLPC.

value, denoted as P_{opt} and determined by the interaction parameters, the device switches to a "closed" state. In this configuration, an incident pseudospin current in the state ψ_- is totally reflected by the effective step potential, emulating the operation of a spintronic spin valve device in its "AP" configuration, as shown in Fig. 6(c). Furthermore, an incident pseudospin of state ψ_+ is transmitted through the device, enabling the routing of different pseudospin states based on their frequency-superposition state.[15]

Another interesting all-optical device is the frequency-superposition beamsplitter (FSBS), which is realized by introducing two synthetic magnetization discontinuities. This device functions similarly to a polarizing beamsplitter but operates on frequency-superposition eigenstates, directing incoming light from one or two spatial input ports to specific output ports based on their frequency-superposition state.[15]

These all-optical devices are highly tunable and scalable, offering rapid optical control via the pump field and enabling fast switching rates for applications such as optical switching. In addition, utilizing quasi-periodic nonlinear photonic crystals,[68,69] these concepts can be extended to higher dimensions, enhancing their versatility in optical signal processing.

E. Pseudospin light guiding in nonlinear photonic crystals

Optical waveguides, based on changes in the linear permittivity, allow confinement and manipulation of light with optical wavelengths. By utilizing the aforementioned analogy, a new waveguide phenomenon was recently introduced, which relies solely on the spatial change of the nonlinear permittivity, using the corresponding spin-1/2 dynamics of SFG in the second-order nonlinear optics.[16,17] Specifically, it allows for exact manipulation of frequency superposition states in a compact and precise manner, all-optically controlled by the pump beam.

In this work, under the quasi-phase-matched condition ($\Delta k = 0$), $M_z = 0$, thus emulating the transverse synthetic magnetization required for realizing simple changing magnetic domains, also

known as spin quantum wells.[70] These dynamics can be described by the following decoupled equations for SFG:

$$i\frac{\partial}{\partial z}\psi_\pm = \left[-\frac{\nabla_T^2}{2k} \mp \mathbf{M}_T(\mathbf{r})\right]\psi_\pm, \tag{12}$$

where $\mathbf{M}_T(\mathbf{r}) = \begin{cases} M_0\,\hat{\mathbf{x}}, & |x| < a \\ 0, & |x| > a \end{cases}$, with a denotes the pseudospin waveguide width. Equation (12) resembles the dynamics of a quantum particle in a potential well for ψ_+, but for ψ_-, it resembles a particle in a potential barrier.

Therefore, a spin quantum well can be reached by transversely varying the duty cycle (here switched between ~0 and ~M_0), switching between different magnetic domains. Namely, the analogy between spin quantum wells and optical waveguides is used to confine light.

Figure 7(a) shows a schematic of the pseudospin waveguide effect, where a strong wide pump shines on a narrow strip of the quasi-phase-matched region. If a narrow idler (or signal) beam focuses on the input facet, it will guide ψ_+ and scatter (and diffract) ψ_-. Figure 7(b) shows a numerical simulation of such a device, where a wide 1064.5 nm pump beam with a waist of 450 μm propagates through the pseudospin waveguide. In addition, the device is excited using a narrow (waist of 30 μm) 1550 nm idler beam. The simulation shows the generated signal beam output facet. Clearly, in the middle, the signal (of ψ_+) is guided in the "X"-axis and diffracted in the "Y"-axis. Next to it is the scattered and diffracted eigenstate.

The results presented in Refs. 16 and 17 show that it is possible to guide waves and build an integrated photonic component without any change in the linear permittivity while borrowing concepts from spintronics. In particular, spin-inspired waveguides bring maximal control to frequency superposition states, which are otherwise extremely hard to manipulate due to dispersion. This may prove critical to advancing spectral domain quantum optics. Moreover, the interaction can be all-optically
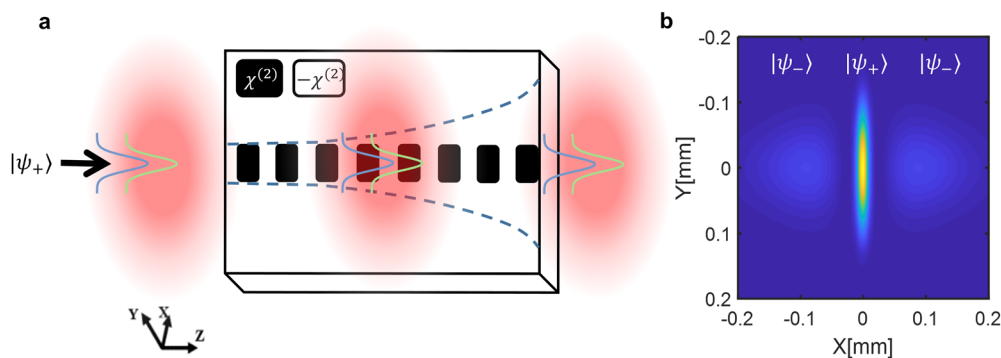
FIG. 7. (a) Schematic of the pseudospin waveguide.[16,17] A narrow idler/signal beam (depicted by two blue/green Gaussians) enters the narrow-poled region, along with a wide strong pump (red Gaussian). A narrow strip of the periodically poled region confines the pseudospin eigenstate, thereby acting as a channel waveguide for both wavelengths with a specific relative phase. The dashed line illustrates regular diffraction of the input beams. (b) Simulation results of the signal output facet. Light in the "X"-axis is confined, while freely propagating in the "Y"-axis. Next to the guided eigenstate is the scattered eigenstate.

controlled by the pump beam, allowing us to envision modular spin-inspired waveguides for classical and quantum optical processing.

IV. SUMMARY AND OUTLOOK

In this article, we reviewed a series of nonlinear optical effects and devices that are inspired by the analogy between the propagation dynamics in a nonlinear mixing process and spin currents in various magnetization textures. The nonlinear processes that we consider are either three-wave mixing in a quadratic nonlinear crystal or FWM in optical fibers. The effects we discussed include the optical Stern–Gerlach effect, the transverse localization of the signal-idler beam in a disordered nonlinear crystal, and the topological Hall effect for light in skyrmionic nonlinear photonic crystals. We also discussed a new class of optical devices that enable splitting, switching, or guiding signal-idler superposition states, depending on their relative phase.

We believe that there are many additional effects and devices that can be studied. Let us briefly mention two future directions. In our analysis, we assumed that the pump (or the two pumps) in the $\chi^{(2)}$ and $\chi^{(3)}$ processes is non-depleted, so that the dynamics is that of a two-mode system. However, when the signal and idler amplitudes become comparable to that of the pump, this assumption is no longer valid, and we reach the fully nonlinear regime where the signal and idler waves will change the pump amplitude. This could lead to a new family of all-optical devices inspired by other spintronic phenomena, such as spin transfer torque,[65] whereby the spin currents alter the material magnetization.

While these effects require high-power signal and idler waves, interesting opportunities also exist in the other extreme range of power, in which these waves contain only single photons. For example, when passing through the optical Stern–Gerlach device, the two photons (one from the signal and one from the idler) will bunch and emerge together in only one of the output ports of the device.[71] This is a manifestation of the Hong–Ou–Mandel (HOM) effect for distinguishable photons. Traditionally, the HOM bunching is observed when indistinguishable photons interfere on a linear beam splitter, but it has been shown that using a set of dichroic mirrors and a nonlinear crystal, bunching can be observed for photons with different frequencies.[72–74] The Stern–Gerlach effect enables observation of this effect in a single nonlinear crystal.[71] Similarly, skyrmionic nonlinear crystals enable the conversion of quantum entanglement between path and spectral degrees of freedom.[14] These methods are not limited only to a pair of frequencies of the signal and idler, and by using multiple pumps and quasiperiodic crystals, they can be extended to multiple waves at different frequencies,[71] thus opening exciting possibilities for manipulation of quantum light in the frequency domain.[75]

Whereas this paper concentrated on using nonlinear optical processes for manipulating light beams, the underlying analogy of spin-1/2 particles in magnetic fields is relevant to many other physical systems. Specifically, the polarization components of optical beams,[27–29,32] or alternatively the complex amplitudes of the electric field in coupled waveguides,[33] can define a spinor that can be manipulated by an analog magnetic field. This was already used to show novel effects such as the Spin-Hall effect or the analog Stern–Gerlach splitting, but it may be further applied to realize new types of spin-dependent devices for guiding and splitting of light waves.

AUTHOR DECLARATIONS

Conflict of Interest

The authors have no conflicts to disclose.

Author Contributions

Gil Bashan, Shani Izhak, and Ofir Yesharim contributed equally to this work.

Gil Bashan: Conceptualization (equal); Formal analysis (equal); Investigation (equal); Methodology (equal); Writing – original draft (equal). **Shani Izhak**: Conceptualization (equal); Formal analysis (equal); Investigation (equal); Methodology (equal); Writing – original draft (equal). **Ofir Yesharim**: Conceptualization (equal); Formal analysis (equal); Investigation (equal); Methodology (equal); Writing – original draft (equal). **Ady Arie**: Conceptualization (equal); Funding acquisition (equal); Project administration (equal); Supervision (equal); Writing – original draft (equal); Writing – review & editing (equal).

DATA AVAILABILITY

The data that support the findings of this study are available from the corresponding author upon reasonable request.

REFERENCES

[1] R. W. Boyd, *Nonlinear Optics*, 3rd ed. (Academic Press, Inc., 2008).

[2] H. Suchowski, D. Oron, A. Arie, and Y. Silberberg, "Geometrical representation of sum frequency generation and adiabatic frequency conversion," Phys. Rev. A **78**, 063821 (2008).

[3] H. Suchowski, G. Porat, and A. Arie, "Adiabatic processes in frequency conversion," Laser Photonics Rev. **8**, 333–367 (2014).

[4] X. Ding, D. Heberle, K. Harrington, N. Flemens, W.-Z. Chang, T. A. Birks, and J. Moses, "Observation of rapid adiabatic passage in optical four-wave mixing," Phys. Rev. Lett. **124**, 153902 (2020).

[5] G. Porat and A. Arie, "Efficient, broadband, and robust frequency conversion by fully nonlinear adiabatic three-wave mixing," J. Opt. Soc. Am. B **30**, 1342–1351 (2013).

[6] A. Karnieli and A. Arie, "Fully controllable adiabatic geometric phase in nonlinear optics," Opt. Express **26**, 4920–4932 (2018).

[7] A. Karnieli, S. Trajtenberg-Mills, G. Di Domenico, and A. Arie, "Experimental observation of the geometric phase in nonlinear frequency conversion," Optica **6**, 1401–1405 (2019).

[8] Y. Li, J. Lü, S. Fu, and A. Arie, "Geometric representation and the adiabatic geometric phase in four-wave mixing processes," Opt. Express **29**, 7288–7306 (2021).

[9] A. Karnieli, Y. Li, and A. Arie, "The geometric phase in nonlinear frequency conversion," Front. Phys. **17**, 12301 (2021).

[10] P. Krogen, H. Suchowski, H. Liang, N. Flemens, K.-H. Hong, F. X. Kärtner, and J. Moses, "Generation and multi-octave shaping of mid-infrared intense single-cycle pulses," Nat. Photonics **11**, 222–226 (2017).

[11] W. Gerlach and O. Stern, "Der experimentelle nachweis der richtungsquantelung im magnetfeld," Z. Phys. **9**, 349–352 (1922).

[12] S. Izhak, A. Karnieli, O. Yesharim, S. Tsesses, and A. Arie, "Pseudospin localization of light in nonlinear optics," in *CLEO 2024* (Optica Publishing Group, 2024), p. FTh3D.3.

[13] S. Izhak, A. Karnieli, O. Yesharim, S. Tsesses, and A. Arie, "Pseudospin transverse localization of light in an optical disordered spin-glass phase," Optica Open. Preprint. (2025).

[14] A. Karnieli, S. Tsesses, G. Bartal, and A. Arie, "Emulating spin transport with nonlinear optics, from high-order skyrmions to the topological hall effect," Nat. Commun. **12**, 1092 (2021).

[15] S. Izhak, A. Karnieli, O. Yesharim, S. Tsesses, and A. Arie, "All-optical spin valve effect in nonlinear optics," Opt. Lett. **49**, 1025–1028 (2024).

[16] O. Yesharim, S. Izhak, and A. Arie, "Light guiding and directional coupling in nonlinear photonic crystals," in *CLEO 2024* (Optica Publishing Group, 2024), p. FF3M.5.

[17] O. Yesharim, S. Izhak, and A. Arie, "Pseudo-spin light circuits in nonlinear photonic crystals," Optica Open. Preprint. (2025).

[18] J. A. Armstrong, N. Bloembergen, J. Ducuing, and P. S. Pershan, "Interactions between light waves in a nonlinear dielectric," Phys. Rev. **127**, 1918–1939 (1962).

[19] J. J. Sakurai and J. Napolitano, *Modern Quantum Mechanics*, 3rd ed. (Cambridge University Press, 2020).

[20] A. Karnieli and A. Arie, "All-optical Stern-Gerlach effect," Phys. Rev. Lett. **120**, 053901 (2018).

[21] The difference in sign between the dispersion and diffraction cases, as indicated by C2, stems from defining the optical frequency as negative. Additionally, for the sake of simplicity, diffraction is represented solely along the x axis, even though it occurs in both axes.

[22] E. H. Kennard, "Zur quantenmechanik einfacher bewegungstypen," Z. Phys. **44**, 326–352 (1927).

[23] E. H. Kennard, "The quantum mechanics of an electron or other particle," J. Franklin Inst. **207**, 47–78 (1929).

[24] G. G. Rozenman, M. Zimmermann, M. A. Efremov, W. P. Schleich, L. Shemer, and A. Arie, "Amplitude and phase of wave packets in a linear potential," Phys. Rev. Lett. **122**, 124302 (2019).

[25] O. Yesharim, A. Karnieli, S. Jackel, G. Di Domenico, S. Trajtenberg-Mills, and A. Arie, "Observation of the all-optical Stern–Gerlach effect in nonlinear optics," Nat. Photonics **16**, 582–587 (2022).

[26] A. Mondal and R. Das, "Experimental evidence of a pump-wavefront-induced Stern–Gerlach-like splitting in optical parametric generators," Opt. Lett. **47**, 3668–3671 (2022).

[27] G. Liu, Z. Zeng, H. Lin, Y. Hu, Z. Li, Z. Chen, and S. Fu, "Electrically engineering synthetic magnetic fields for polarized photons," Optica **11**, 980–987 (2024).

[28] K. Y. Bliokh, A. Niv, V. Kleiner, and E. Hasman, "Geometrodynamics of spinning light," Nat. Photonics **2**, 748–753 (2008).

[29] K. Y. Bliokh, F. J. Rodríguez-Fortuño, F. Nori, and A. V. Zayats, "Spin–orbit interactions of light," Nat. Photonics **9**, 796–808 (2015).

[30] X. Liu, S. Xia, E. Jajtić, D. Song, D. Li, L. Tang, D. Leykam, J. Xu, H. Buljan, and Z. Chen, "Universal momentum-to-real-space mapping of topological singularities," Nat. Commun. **11**, 1586 (2020).

[31] J. Wang, L. Shi, and J. Zi, "Spin hall effect of light via momentum-space topological vortices around bound states in the continuum," Phys. Rev. Lett. **129**, 236101 (2022).

[32] W. Zhu, X. Liang, X. Xie, H. Zheng, Y. Zhong, J. Tang, J. Yu, and Z. Chen, "Optical Stern–Gerlach effect in periodically poled electro-optical crystals," Laser Photonics Rev. **18**, 2301030 (2024).

[33] J. Li, Z. Wang, Y. Hu, and J. Xu, "Splitting of optical spatial modes via Stern-Gerlach effect," Laser Photonics Rev. **18**, 2301055 (2024).

[34] G. Bashan, A. Eyal, M. Tur, and A. Arie, "All-optical Stern-Gerlach Effect in the time domain," Opt. Express **32**, 9589–9601 (2024).

[35] S. F. Edwards and P. W. Anderson, "Theory of spin glasses," J. Phys. F: Met. Phys. **5**, 965 (1975).

[36] M. B. Weissman, "What is a spin glass? A glimpse via mesoscopic noise," Rev. Mod. Phys. **65**, 829–839 (1993).

[37] G. Parisi, "Spin glasses and fragile glasses: Statics, dynamics, and complexity," Proc. Natl. Acad. Sci. U. S. A. **103**, 7948–7955 (2006).

[38] M. Mezard, G. Parisi, and M. Virasoro, *Spin Glass Theory and Beyond* (World Scientific, 1986).

[39] D. Venturelli, S. Mandrà, S. Knysh, B. O'Gorman, R. Biswas, and V. Smelyanskiy, "Quantum optimization of fully connected spin glasses," Phys. Rev. X **5**, 031040 (2015).

[40] C. Fan, M. Shen, Z. Nussinov, Z. Liu, Y. Sun, and Y.-Y. Liu, "Searching for spin glass ground states through deep reinforcement learning," Nat. Commun. **14**, 725 (2023).

[41] S. H. Skjærvø, C. H. Marrows, R. L. Stamps, and L. J. Heyderman, "Advances in artificial spin ice," Nat. Rev. Phys. **2**, 13–28 (2019).

[42] K. Binder and A. P. Young, "Spin glasses: Experimental facts, theoretical concepts, and open questions," Rev. Mod. Phys. **58**, 801–976 (1986).

[43] P.-E. Wolf and G. Maret, "Weak localization and coherent backscattering of photons in disordered media," Phys. Rev. Lett. **55**, 2696–2699 (1985).

[44] M. P. V. Albada and A. Lagendijk, "Observation of weak localization of light in a random medium," Phys. Rev. Lett. **55**, 2692–2695 (1985).

[45] P. W. Anderson, "Absence of diffusion in certain random lattices," Phys. Rev. **109**, 1492–1505 (1958).

[46] A. Lagendijk, B. v. Tiggelen, and D. S. Wiersma, "Fifty years of Anderson localization," Phys. Today **62**(8), 24–29 (2009).

[47] T. Schwartz, G. Bartal, S. Fishman, and M. Segev, "Transport and Anderson localization in disordered two-dimensional photonic lattices," Nature **446**, 52–55 (2007).

[48] Y. Lahini, A. Avidan, F. Pozzi, M. Sorel, R. Morandotti, D. N. Christodoulides, and Y. Silberberg, "Anderson localization and nonlinearity in one-dimensional disordered photonic lattices," Phys. Rev. Lett. **100**, 013906 (2008).

[49] H. De Raedt, A. Lagendijk, and P. de Vries, "Transverse localization of light," Phys. Rev. Lett. **62**, 47–50 (1989).

[50] A. Mafi, "Transverse Anderson localization of light: A tutorial," Adv. Opt. Photonics **7**, 459–515 (2015).

[51] M. Segev, Y. Silberberg, and D. N. Christodoulides, "Anderson localization of light," Nat. Photonics **7**, 197–204 (2013).

[52] N. Hanasaki, K. Watanabe, T. Ohtsuka, I. Kézsmárki, S. Iguchi, S. Miyasaka, and Y. Tokura, "Nature of the transition between a ferromagnetic metal and a spin-glass insulator in pyrochlore molybdates," Phys. Rev. Lett. **99**, 086401 (2007).

[53] G. Tarnopolsky, C. Li, D. G. Joshi, and S. Sachdev, "Metal-insulator transition in a random Hubbard model," Phys. Rev. B **101**, 205106 (2020).

[54] J. B. Goodenough, R. I. Dass, and J. Zhou, "Spin-glass to ferromagnet transition in $LaMn_{1-x}Sc_xO_3$," Solid State Sci. **4**, 297–304 (2002).

[55] S. Mühlbauer, B. Binz, F. Jonietz, C. Pfleiderer, A. Rosch, A. Neubauer, R. Georgii, and P. Böni, "Skyrmion lattice in a chiral magnet," Science **323**, 915–919 (2009).

[56] K. Everschor-Sitte and M. Sitte, "Real-space berry phases: Skyrmion soccer (invited)," J. Appl. Phys. **115**, 172602 (2014).

[57] Y. Shen, Q. Zhang, P. Shi, L. Du, X. Yuan, and A. V. Zayats, "Optical skyrmions and other topological quasiparticles of light," Nat. Photonics **18**, 15–25 (2024).

[58] S. Tsesses, E. Ostrovsky, K. Cohen, B. Gjonaj, N. H. Lindner, and G. Bartal, "Optical skyrmion lattice in evanescent electromagnetic fields," Science **361**, 993–996 (2018).

[59] L. Du, A. Yang, A. V. Zayats, and X. Yuan, "Deep-subwavelength features of photonic skyrmions in a confined electromagnetic field with orbital angular momentum," Nat. Phys. **15**, 650–654 (2019).

[60] T. J. Davis, D. Janoschka, P. Dreher, B. Frank, F.-J. Meyer zu Heringdorf, and H. Giessen, "Ultrafast vector imaging of plasmonic skyrmion dynamics with deep subwavelength resolution," Science **368**, eaba6415 (2020).

[61] S. Gao, F. C. Speirits, F. Castellucci, S. Franke-Arnold, S. M. Barnett, and J. B. Götte, "Paraxial skyrmionic beams," Phys. Rev. A **102**, 053513 (2020).

[62] D. A. Smirnova, F. Nori, and K. Y. Bliokh, "Water-wave vortices and skyrmions," Phys. Rev. Lett. **132**, 054003 (2024).

[63] B. Wang, Z. Che, C. Cheng, C. Tong, L. Shi, Y. Shen, K. Y. Bliokh, and J. Zi, "Topological water-wave structures manipulating particles," arXiv:2406.08515 [physics.class-ph] (2024).

[64] Y. Zhang, Y. Sheng, S. Zhu, M. Xiao, and W. Krolikowski, "Nonlinear photonic crystals: From 2D to 3D," Optica **8**, 372–381 (2021).

[65] J. C. Sankey, Y.-T. Cui, J. Z. Sun, J. C. Slonczewski, R. A. Buhrman, and D. C. Ralph, "Measurement of the spin-transfer-torque vector in magnetic tunnel junctions," Nat. Phys. **4**, 67–71 (2008).

[66] B. Dieny, V. Speriosu, B. Gurney, S. Parkin, D. Wilhoit, K. Roche, S. Metin, D. Peterson, and S. Nadimi, "Spin-valve effect in soft ferromagnetic sandwiches," J. Magn. Magn. Mater. **93**, 101–104 (1991).

[67] S. Bhatti, R. Sbiaa, A. Hirohata, H. Ohno, S. Fukami, and S. Piramanayagam, "Spintronics based random access memory: A review," Mater. Today **20**, 530–548 (2017).

[68] A. Arie and N. Voloch, "Periodic, quasi-periodic, and random quadratic nonlinear photonic crystals," Laser Photonics Rev. **4**, 355–373 (2010).

[69] A. Bahabad, A. Ganany-Padowicz, and A. Arie, "Engineering two-dimensional nonlinear photonic quasi-crystals," Opt. Lett. **33**, 1386–1388 (2008).

[70] V. K. Dugaev, J. Barnaś, and J. Berakdar, "Electrons in ferromagnets with domain walls," J. Phys. A: Math. Gen. **36**, 9263 (2003).

[71] A. Karnieli and A. Arie, "Frequency domain Stern–Gerlach effect for photonic qubits and qutrits," Optica **5**, 1297–1303 (2018).

[72] T. Kobayashi, R. Ikuta, S. Yasui, S. Miki, T. Yamashita, H. Terai, T. Yamamoto, M. Koashi, and N. Imoto, "Frequency-domain Hong–Ou–Mandel interference," Nat. Photonics **10**, 441–444 (2016).

[73] P. Imany, O. D. Odele, M. S. Alshaykh, H.-H. Lu, D. E. Leaird, and A. M. Weiner, "Frequency-domain sdel interference with linear optics," Opt. Lett. **43**, 2760–2763 (2018).

[74] C. Joshi, A. Farsi, A. Dutt, B. Y. Kim, X. Ji, Y. Zhao, A. M. Bishop, M. Lipson, and A. L. Gaeta, "Frequency-domain quantum interference with correlated photons from an integrated microresonator," Phys. Rev. Lett. **124**, 143601 (2020).

[75] H.-H. Lu, M. Liscidini, A. L. Gaeta, A. M. Weiner, and J. M. Lukens, "Frequency-bin photonic quantum information," Optica **10**, 1655–1671 (2023).